THE PROTEIN SOCIETY

Advanced analyses of kinetic stabilities of IgGs modified by mutations and glycosylation

Erik Sedlák,[1,2,3] Jonas V. Schaefer,[1] Jozef Marek,[4] Peter Gimeson,[5] and Andreas Plückthun[1]*

[1]Department of Biochemistry, University of Zurich, Winterthurerstrasse 190, CH-8057 Zurich, Switzerland
[2]Centre for Interdisciplinary Biosciences, P.J. Šafárik University, Moyzesova 11, Košice 040 01, Slovakia
[3]Department of Biochemistry, P.J. Šafárik University, Moyzesova 11, Košice 040 01, Slovakia
[4]Department of Biophysics, Institute of Experimental Physics, Watsonova 47, Košice 040 01, Slovakia
[5]Malvern Instruments Inc., Northampton, Massachusetts, 01060-2327, USA

Received 26 February 2015; Accepted 29 April 2015
DOI: 10.1002/pro.2691
Published online 13 May 2015 proteinscience.org

Abstract: The stability of Immunoglobulin G (IgG) affects production, storage and usability, especially in the clinic. The complex thermal and isothermal transitions of IgGs, especially their irreversibilities, pose a challenge to the proper determination of parameters describing their thermodynamic and kinetic stability. Here, we present a reliable mathematical model to study the irreversible thermal denaturations of antibody variants. The model was applied to two unrelated IgGs and their variants with stabilizing mutations as well as corresponding non-glycosylated forms of IgGs and Fab fragments. Thermal denaturations of IgGs were analyzed with three transitions, one reversible transition corresponding to C_H2 domain unfolding followed by two consecutive irreversible transitions corresponding to Fab and C_H3 domains, respectively. The parameters obtained allowed us to examine the effects of these mutations on the stabilities of individual domains within the full-length IgG. We found that the kinetic stability of the individual Fab fragment is significantly lowered within the IgG context, possibly because of intramolecular aggregation upon heating, while the stabilizing mutations have an especially beneficial effect. Thermal denaturations of non-glycosylated variants of IgG consist of more than three transitions and could not be analyzed by our model. However, isothermal denaturations demonstrated that the lack of glycosylation affects the stability of all and not just of the C_H2 domain, suggesting that the partially unfolded domains may interact with each other during unfolding. Investigating thermal denaturation of IgGs according to our model provides a valuable tool for detecting subtle changes in thermodynamic and/or kinetic stabilities of individual domains.

Keywords: differential scanning calorimetry; irreversible transition; multidomain protein; IgG stability; half-life; kinetic stability

Abbreviations used: ANS, 8-anilinonaphthalene-1-sulfonate; C_H, constant domain of the heavy chain; C_L, constant domain of the light chain; DSC, differential scanning calorimetry; GdmCl, guanidinium chloride; IgG, immunoglobulin G; ITF, intrinsic tryptophan fluorescence; PBS, phosphate-buffered saline; SAXS, small-angle X-ray scattering; WT, wild type; M, mutant.

Additional Supporting Information may be found in the online version of this article

Erik Sedlák and Jonas V. Schaefer contributed equally to this work.

Grant sponsor: Slovak Grant Agency VEGA; Grant number: 1/0521/12; Grant sponsor: FP7 EU Programs REGPOT and PCUBE; Grant sponsor: FP7 EU Regional Potential; Grant number: 316310.

*Correspondence to: Andreas Plückthun, Department of Biochemistry, University of Zurich, Winterthurerstrasse 190, CH-8057 Zurich, Switzerland. E-mail: plueckthun@bioc.uzh.ch

Introduction

Immunoglobulins (IgGs) are structurally rather complex molecules. They consist of four polypeptide chains containing multiple intra- and interchain disulfide bonds. The structure of immunoglobulins is composed of a total of 12 domains that interact in a pair-wise fashion, thus forming four heterodimeric and two homodimeric "super-domains" (Fig. 1). These domains can be grouped together in different segments: the two identical antigen-binding Fab fragments are connected via the hinge region with the Fc fragment responsible for the molecule's effector functions—forming the well-known Y-shaped conformation. One of these homodimeric domains in the Fc fragment, namely the C_H2 domains, is generally glycosylated at asparagine 297, and the contacts between the domains are entirely mediated by the sugars.

Immunoglobulins are very promising candidates in the development of new drugs with many of them already being used successfully in the clinic.[1] One of the most important biophysical parameters characterizing these molecules is their stability. In fact, comprehensive knowledge about factors determining or even predicting protein stability in general would clearly facilitate the development of optimal protein frameworks, production conditions as well as solvent formulations. In principle, there are two types of stabilities that need to be taken into consideration: the *thermodynamic* stability, dealing with equilibrium transitions and describing the stability of the protein as its free energy of unfolding as a function of temperature, as well as the *kinetic* stability, reflecting irreversible transitions and specifying the stability of the protein as a function of time (determined by rate constant of a rate-limiting irreversible step) with temperature as a parameter.[2–4] This kinetic stability can not only determine the shelf-life, but also the in vivo performance of an antibody.

The simplest model describing the thermodynamic stability of a given protein is the two-state model, where the native state (N) is in equilibrium with the denatured state (D): $N \overset{K}{\rightleftharpoons} D$ with K being the equilibrium constant of the reaction. In such a case, removal of denaturation conditions (temperature, chemical denaturants, etc.) causes a shift of the equilibrium toward the N state. Thus, theoretically, the so called half-life of a reversibly unfolding protein is unlimited.

The simplest model for describing the kinetic stability, on the other hand, is a particular case of the Lumry-Eyring model[5]: $N \overset{K}{\rightleftharpoons} D \overset{k}{\longrightarrow} F$ that can be simplified by the following equation: $N \overset{k'}{\longrightarrow} F$, where F is the final (denatured) state of the protein, and k and k' are the rate constants of the irreversible steps of this reaction (determining the theoretical half-life of the protein under the given conditions).

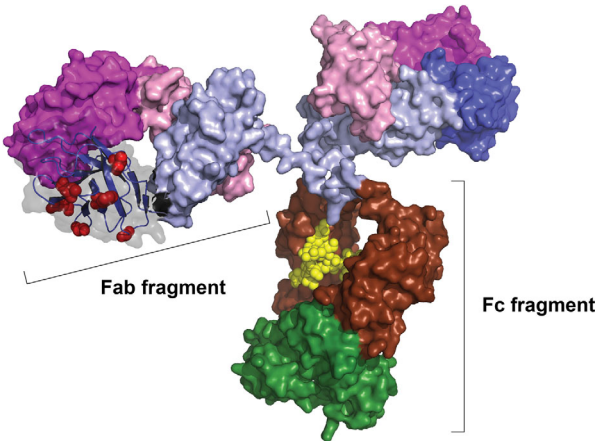

Figure 1. Structure of analyzed IgGs, having the well-known Y-shaped conformation. Both the Fab as well as the Fc fragment are labeled. Individual domains are shown as differently colored surfaces: V_H is represented in dark blue, C_H1 in light blue, C_H2 in brown, C_H3 in green, V_L in magenta and C_L in pink. The six stabilizing mutations are highlighted within one transparent V_H domain as red spheres, the glycan moieties of the C_H2 domains are shown in yellow.

In thermal or denaturant-induced denaturations of multidomain proteins such as IgGs, several overlapping transitions—often involving irreversible steps—have to be considered for the determination of the protein's thermal stability. Numerous studies highlight the power of differential scanning calorimetry (DSC) as the method of choice for studying these multidomain proteins.[6–8] The major advantage of DSC is its ability to usually discernibly distinguish transitions that are difficult to detect and to differentiate by other methods, such as spectroscopic approaches. This is especially important for the analyses of immunoglobulins, as their thermal transitions consist of two or three peaks that can be ascribed to the reversible denaturation of C_H2 domains, the cooperatively irreversible denaturation of the Fab fragments and the cooperatively irreversible denaturation of the C_H3 domains.[9]

Numerous studies on the thermal denaturation of IgGs have been performed, reporting effects of pH,[10–15] formulation,[16,17] as well as the cooperativity within the IgG molecules.[9,10,18,19] Despite the absence of relevant information regarding the number and reversibility of studied transitions, in all these studies thermal transitions of IgGs were analyzed based on deconvolutions using equilibrium transitions. This approach is, however, questionable as the thermal transitions (besides the homodimeric domain C_H2) of IgGs are irreversible and thus kinetically driven. Although it has been shown that the thermal denaturation of several proteins, under certain circumstances, can be interpreted in terms of the van't Hoff equation despite their calorimetric irreversibility,[20–22] the irreversibility and

dependence of thermal denaturation on the used scan rate exclude IgGs from this category.

In the present work, we have created a model and derived appropriate equations that reliably describe all transitions present. As a proof of principle, we applied this model to stability analyses of IgGs with known, well-characterized properties. The obtained results also incorporate kinetic stability data and indicate, partly in contrast to previously published data, that domains "feel" the presence of their neighboring domains, possibly by partially unfolded domains interacting with each other. This is reflected in the interdependence of parameters describing thermal denaturation of IgG variants. This conclusion is further supported by additional results obtained from isothermal denaturation experiments.

Material and Methods

Purification of IgGs

Antibodies were expressed and purified from mammalian cell culture supernatants as described previously.[23] Briefly, the supernatants were loaded onto HiTrap Protein A columns (GE Healthcare) at 4°C at a flow rate of 1 mL/min. Chromatography was performed using an ÄKTA PrimePlus chromatography system (GE Healthcare) at 4°C. After loading, the column was washed with 100 m*M* sodium phosphate buffer pH 8.0 containing 150 m*M* NaCl. Elution of IgG was accomplished by using 100 m*M* glycine pH 2.7, followed by immediate neutralization of each fraction to pH 7.5 using 1*M* Tris, pH 8.0. The concentrations of the sample fractions were determined by UV-spectroscopy at 280 nm with a NanoDrop ND-1000 spectrophotometer (Thermo Scientific), assuming a mass extinction coefficient of 1.37 for a 1 mg/mL solution of IgG. The samples with the highest protein concentration were pooled and dialyzed twice against PBS (Sigma-Aldrich; 10 m*M* Na_2HPO_4, 1.8 m*M* KH_2PO_4, 2.7 m*M* KCl, 137 m*M* NaCl, pH 7.1) at 4°C. After dialysis, the samples were filtered through 0.22 μm filters (Millipore) and stored at 4°C.

Guanidinium chloride-induced equilibrium unfolding measured by intrinsic tryptophan fluorescence (ITF)

Guanidinium chloride (GdmCl)-induced denaturation measurements were carried out with protein/GdmCl mixtures containing a final protein concentration of 1 μM and denaturant concentrations ranging from 0 to 5*M* (99.5% purity, Fluka, MO). These mixtures were prepared from a 6*M* GdmCl stock solution (in PBS, pH adjusted to 7.1) and equilibrated for up to 7 days at 25°C. Each final concentration of GdmCl was determined by measuring the refractive index. The intrinsic fluorescence emission spectra were then recorded from 300 to 400 nm with an excitation wavelength of 295 nm in an Infinite M1000 reader (Tecan, NC). Individual GdmCl blanks were recorded and automatically subtracted from the data.

ANS measurements

Samples of different antibody formats were mixed with 200 μ*M* 8-anilino-naphthalene-1-sulfonic acid (ANS) and incubated for 7 days at room temperature. The fluorescence emission spectra were recorded from 430 to 550 nm with an excitation wavelength of 390 nm in an Infinite M1000 reader (Tecan, NC) and averaged over 10 accumulations.

Differential scanning calorimetry

DSC measurements were performed using a VP-Capillary DSC system (Microcal, acquired by Malvern Instruments Ltd). The antibody concentrations were adjusted to 0.5 mg/mL before the measurement unless otherwise stated. The corresponding buffer was used as a reference. The samples were heated from 15°C to 100°C at the stated rates after initial 8 min of equilibration at 15°C. A filtering period of 10 s was used and data were analyzed using Origin 7.0 software (OriginLab Corporation, MA). Thermograms were corrected by subtraction of buffer-only scans and then normalized to the molar concentration of the protein.

Analysis of DSC scans

The experimental data of the excess heat capacity of IgG obtained from DSC were fitted by Eq. (A14) (see Appendix). The experimental data of the excess heat capacity of Fab fragments were fitted by Eq. (4). DSC data were analyzed by numerical analysis in Microsoft Excel® by nonlinear regression using the Solver Add-in. Regression statistics for regression coefficients (the standard deviations of the regression coefficients and R^2), obtained by using the Solver Add-in, were calculated by utilizing the SolvStat Add-in.

Results

For analyzing the stability aspects of various formats and constructs, we chose a set of already well-characterized antibodies, IgG6B3 and IgG2C2, that contain the same heavy chain subclass (V_H6) but dissimilar light chains, $V_\kappa3$ in IgG2C2 and $V_\lambda3$ in IgG6B3.[23,24] Next to the original IgG (WT for wild type), an engineered variant with framework mutations in V_H (M for mutant) of the otherwise identical IgG, displaying improved biophysical properties, was analyzed as well. All point mutations present in the engineered antibodies (Q5V, S16G, T58I, V72D, S76G, and S90Y) are located outside the CDRs in the V_H framework (Fig. 1), and thus in the Fab fragment of the IgG.

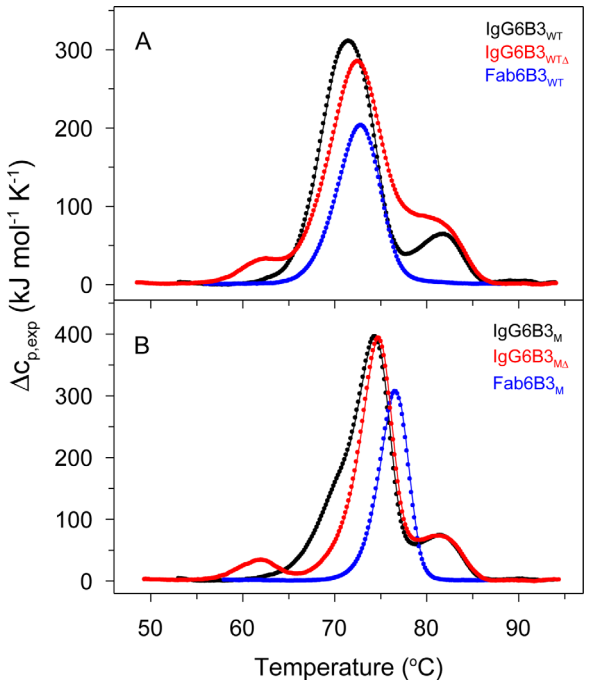

Figure 2. Thermal denaturation of different antibody IgG6B3 formats monitored by DSC. (A) IgG6B3$_{WT}$ (black), Fab6B3$_{WT}$ (blue), and IgG6B3$_{WT\Delta}$ (red); (B) IgG6B3$_{M}$ (black), Fab6B3$_{M}$ (blue), and IgG6B3$_{M\Delta}$ (red). In all cases, DSC experiments were performed with 0.5 mg/mL of protein in PBS buffer, pH 7.4 at a scan rate of 1.0 K/min.

Effect of the mutations and of a lack of glycosylation on thermal stability of antibodies

The effect of the mutations and lack of glycosylation on the thermal stability of IgG6B3 and Fab6B3 variants was assessed by DSC experiments (Fig. 2). As previously shown, the six point mutations present in the V_H domain of the engineered antibodies have a stabilizing effect on both the Fab6B3 fragment as well as the whole IgG6B3 molecule (Fig. 2).[23] While thermal denaturation of the whole IgG6B3 is at least a two-step process (as indicated by two peaks), DSC scans of the Fab6B3 fragment consist of only one peak, indicating a one-step transition. The stabilization effect of the mutations on the Fab6B3 fragment is apparent from the shift of the transition temperature, T_{trs}, of Fab6B3$_{WT}$ from 72.8°C to 76.5°C measured for Fab6B3$_{M}$. This improved stability also holds true within the IgG6B3 context. The DSC profile of thermal transition of IgG6B3$_{WT}$ consists of a high and broad peak at T_{trs} = 71.5°C followed by a small peak at T_{trs} = 81.8°C [Fig. 2(A)]. The mutations in IgG6B3$_{M}$ cause two apparent changes to the thermal transitions of IgG6B3: (i) the first peak becomes asymmetric with a shoulder at the leading side of the peak, and (ii) the main transition shifts to higher temperature with T_{trs} = 74.4°C. The position and apparent enthalpy of the subsequent transition at T_{trs}~82°C is unaffected by the mutations (Fig. 2).

The effect of absence of glycosylation on protein stability was investigated with glycan-knock-outs of IgG, referred to as IgG$_{WT\Delta}$ and IgG$_{M\Delta}$, respectively. These variants do not possess the NxT motif, responsible for N-linked glycosylation at Asn297, due to replacement of threonine at position 299 by alanine.[23] In both non-glycosylated forms of IgG6B3 (WT and M), the lack of glycosylation is accompanied by an appearance of an additional transition at ~62°C (Fig. 2). Both forms thus undergo now three distinct thermally induced transitions: IgG6B3$_{WT\Delta}$ at T_{trs}~62°C, ~72.5°C, ~82°C and IgG6B3$_{M\Delta}$ at T_{trs}~62°C, ~74.5°C, ~82°C. The existence of three transitions in thermal denaturation of IgG is in agreement with previously published findings, stating that thermal denaturation of immunoglobulins proceeds through three subsequent transitions, corresponding (from low to high temperatures) to (i) the C_H2 domains, (ii) the Fab fragment, and finally (iii) C_H3 domains.[9,25,26]

Detailed analyses of thermal denaturation of the studied antibodies showed that their thermal denaturations are both scan-rate-dependent (Fig. 3) and become irreversible upon heating to ~90°C (data not shown). Thermally denatured antibodies are incapable to properly refold due to their aggregation in the process of thermal denaturation.[27] Interestingly, the thermal transitions are, however, independent of protein concentration, as even a 10-fold increase (from 0.25 to 2.5 mg/mL) in protein concentration has no apparent effect on DSC chromatograms (Supporting Information Fig. S1). The observed lack of dependence of the transition temperature on protein concentration indicates that the oligomerization/aggregation is not part of the rate-limiting irreversible reaction.[5,28] Furthermore, the aggregation reaction may involve intramolecular associations of partially unfolded domains.

Model of thermal denaturation of IgG

Closer analyses of individual thermally induced transitions of the whole IgG (studied in this work) and analogous IgGs (unpublished data) show that the first transition, corresponding to the C_H2 domains, is reversible, in agreement with previously published findings.[29] However, this holds true only when heating is stopped during or right after the first transition (~72°C for glycosylated IgGs) and the sample is (quickly) re-cooled to pre-transition temperatures. If the protein is held at post-transition temperatures (of the first transition) for too long and/or the heating continues to higher temperatures, the transition becomes irreversible as well.

Thermal denaturation of IgG based on analyses of numerous IgGs can be described by three consecutive transitions (one reversible followed by two irreversible transitions) and is expressed by Eq. (1):

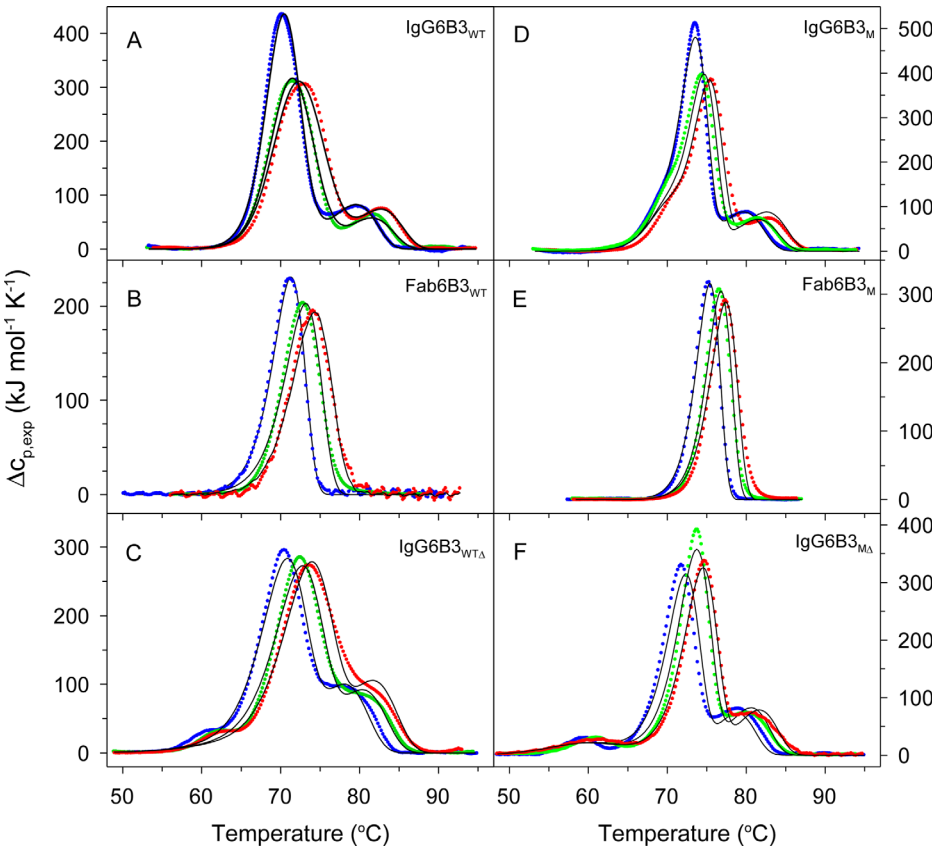

Figure 3. Thermal denaturations of IgG6B3s and Fab6B3 fragments as a function of scan rate monitored by DSC: Data from (A) IgG6B3$_{WT}$, (B) Fab6B3$_{WT}$, (C) IgG6B3$_{WT\Delta}$, (D) IgG6B3$_{M}$, (B) Fab6B3$_{M}$, (C) IgG6B3$_{M\Delta}$ indicate that these proteins are under kinetic control. Measurements were performed at three different scan rates: 0.5 K/min (blue), 1.0 K/min (green), and 1.5 K/min (red). Experimental data are shown as dots; theoretical fits based on a global fit according to Eq. (3) for IgGs (boxes A, C, D, and F) and to Eq. (4) for Fab (B and E) are shown as solid lines. In all cases, DSC experiments were performed with 0.5 mg/mL of protein in PBS buffer, pH 7.4.

$$N \overset{K}{\rightleftharpoons} U \xrightarrow{k_2} D \xrightarrow{k_3} F \tag{1}$$

where N is the native state, U and D are intermediate states of thermal denaturation and F is the final (denatured) state of IgG; K is the equilibrium constant of the first transition, k_2 and k_3 are rate constants of the corresponding irreversible reactions. The excess heat capacity, which is the parameter measured in the DSC experiments, is expressed by the general equation satisfying the model:

$$C_p^{excess}(T) = -\Delta H_1\left(\frac{dn_N}{dT}\right) + \Delta H_2\left(\frac{k_2 n_U}{v}\right) + \Delta H_3\left(\frac{k_3 n_D}{v}\right) \tag{2}$$

where ΔH_1, ΔH_2, and ΔH_3 are molar enthalpy changes for the first, second and third steps, respectively; n_N, n_U, and n_D are molar fractions of corresponding states of the protein and v is the scan rate in K/min. Substitution of molar fractions by derived equations (see Appendix) leads to the equation:

$$\begin{aligned} C_p^{excess}(T) = {} & \Delta H_1 \frac{K}{(K+1)^2}\left(\frac{k_2}{v} + \frac{\Delta H_1}{RT^2}\right)\varepsilon_K \\ & + \Delta H_2 \frac{K}{K+1}\left(\frac{k_2}{v}\right)\varepsilon_K + \Delta H_3 \frac{k_3}{v^2}\varepsilon_3 \int\left(\frac{k_2 K}{K+1}\frac{\varepsilon_K}{\varepsilon_3}\right)dT \end{aligned} \tag{3}$$

where

$$K = \frac{k_1}{k_{-1}} = exp\left(-\frac{\Delta H_1}{R}\left(\frac{1}{T} - \frac{1}{T_{1/2}}\right)\right)$$

$$k_2 = exp\left(-\frac{E_{a2}}{R}\left(\frac{1}{T} - \frac{1}{T_2^*}\right)\right)$$

$$k_3 = exp\left(-\frac{E_{a3}}{R}\left(\frac{1}{T} - \frac{1}{T_3^*}\right)\right)$$

$$\varepsilon_K = exp\left(-\frac{1}{v}\int\frac{k_2 K}{K+1}dT\right)$$

$$\varepsilon_3 = exp\left(-\frac{1}{v}\int k_3 dT\right)$$

Detailed description of the derivation of Eq. (3) is provided in the Appendix.

For fitting the thermal transition of Fab fragments consisting only of a one-step irreversible transition, the following equation was used[5,30]:

$$C_p^{excess} = \frac{\Delta H_2 k_2}{v} exp\left(-\frac{1}{v}\int k_2 dT\right) \quad (4)$$

where the fitting parameters have the same meaning as defined above. The subscript 2 is used to highlight that the description of this thermal denaturation is in agreement with the description of this step within the whole IgG molecule (refer to Eq. (1)).

Analysis of thermal denaturation of the proteins

The DSC scans of IgG6B3 and Fab6B3 were analyzed by using Eqs. (3) and (4), respectively. Fits were excellent in most cases. Fitting parameters of individual fits are listed in Table S1 in the Supporting information. However, in order for the model to be an adequate description of the thermal denaturation, there must be consistency between the fits achieved for the DSC profiles obtained at different scan rates. The data were therefore fitted globally, that is, parameters characterizing the reversible transition such as ΔH (calorimetric enthalpy) and $T_{1/2}$ (transition temperature) as well as the parameters of the irreversible steps like E_a (activation energy) and T^* (temperature at which the rate of an irreversible step is equal 1 min^{-1}) were forced to be the same for all scan rates. Fitting parameters obtained from global fits are listed in Table I and the fits are shown in Figure 3. These fits are in very good agreement with the experimental data (based on correlation coefficients as well as on visual inspection) for all IgGs and Fab fragments, thus indicating thus a robustness of the model. Interestingly, they are consistently worse for the non-glycosylated counterparts of IgGs, suggesting that the thermal denaturation of non-glycosylated IgG is more complex than the derived model, potentially containing additional irreversible steps.

Fitting parameters obtained from thermal denaturations of $Fab6B3_{WT}$ and $Fab6B3_M$ unambiguously show the stabilization effect of the mutations (Table I). Both parameters characterizing the rate constant, that is, T^* and E_a, increased by 2.5°C and ~200 kJ/mol, respectively. The increase in these parameters results in a ~10'000-fold increase in kinetic stability, expressed as the "half-life" of the Fab fragment at 37°C, calculated as $\tau = ln2/k_2$. Interestingly, the mutations have even a higher relative kinetic stabilization effect when the Fab fragment is part of the whole IgG. While this is not apparent in the very similar T_2^*, the activation energy E_{a2} of the Fab fragment in the IgG context appears higher (Table I). A treatment of this step as a reversible transition would thus not notice the change within the Fab fragment, but the measurements at different scan rates have uncovered this. While indeed the Fab fragment is separated from the Fc part and from the other Fab fragment by the hinge region, the partially denatured Fab fragments may aggregate with each other for the wild type, but less so for the mutant, making the differentiation between wild type and mutant much larger than for the Fab fragment. This hypothesis of an intramolecular "aggregation" upon heating within the IgG is also consistent with the lack of concentration dependence (Supporting Information Fig. S1). The calculated half-life for the $IgG6B3_{WT}$ is ~3 days at 37°C, while the kinetic stability of IgG_M is increased by 6 orders of magnitude.

The model was also applied in the analyses of thermal denaturations of an unrelated antibody, $IgG2C2_{WT}$ and its variant $IgG2C2_M$, containing the same mutations as $IgG6B3_{WT}$ (Fig. 4).[23] The thermal denaturations of both $IgG2C2_{WT}$ and $IgG2C2_M$ are scan-rate-dependent and proceed in three steps, a first reversible transition followed by two irreversible transitions, in accordance with the model shown in Eq. (1). Analogously, as in the case of IgG6B3, the fits are in very good agreement with experimental data of IgG2C2 (Fig. 4). Comparison of the fitting parameters for individual scans of $IgG2C2_{WT}$ and $IgG2C2_M$ (Supporting Information Table S1) as well as the global fits (Table I) show that the mutations in the context of IgG2C2 have a similar stabilizing effect (although about 1 order of magnitude lower than in the context of IgG6B3).

Thermal denaturations of $IgG2C2_{WT\Delta}$ and $IgG2C2_{M\Delta}$ show a more complex process than for their glycosylated variants. The non-glycosylated variants of IgG2C2 undergo thermal denaturation in, at least, 4 steps that are clearly distinguishable in $IgG2C2_M$. Therefore, the derived model cannot be applied for the analysis of thermal denaturations of non-glycosylated IgG2C2 variants.

Isothermal chemical denaturation of antibodies

An alternative way to address protein stability is by isothermal chemical denaturation, usually performed by denaturants such as GdmCl or urea. However, to be able to extract proper thermodynamic parameters (such as ΔG_{H2O} values) for a given protein, its denaturation has to be reversible and in general should not consist of more than two steps. In fact, when isothermal denaturation of a protein proceeds through more than two steps, the obtained fits are usually unreliable due to unresolved, overlapping transitions and/or the presence of "hidden" intermediate states of the protein. Unfortunately, IgGs as well as Fab fragments consist of several similar domains that unfold irreversibly at similar denaturant concentrations. Despite the unsuitable properties of these proteins, we were

Table I. *Fitting Parameters for Thermal Transitions of IgGs and Fab Fragments Obtained From Global Fits of Experimental Data to Eqs. (3) and (4), Respectively*

Protein	$T_{1/2}$ (°C)	ΔH_1 (kJ/mol)	T_2^* (°C)	E_{a2} (kJ/mol)	Half-life factor[a]	T_3^* (°C)	E_{a3} (kJ/mol)
$IgG6B3_{WT}$	69.9	517	76.1	202	1	84.9	348
$IgG6B3_{M}$	69.9	584	75.7	542	2×10^6	84.5	358
$Fab6B3_{WT}$	n.a.	n.a.	75.2	427	1×10^4	n.a.	n.a.
$Fab6B3_{M}$	n.a.	n.a.	77.7	615	1×10^8	n.a.	n.a.
$IgG2C2_{WT}$	69.7	480	88.8	106	0.05	88.5	325
$IgG2C2_{M}$	69.6	632	86.7	294	1×10^4	90.0	357

[a] The half-life factor is expressed as approximate factors relative to the half-life of $IgG6B3_{WT}$ at 37°C.
n.a. – not applicable.

interested in whether their isothermal denaturations are affected by mutations and/or the lack of glycosylation. Although the obtained results can be considered to be only of qualitative nature, they show stabilization effects for mutations and the glycosylated state of the analyzed IgG6B3s (Fig. 5) as described in the following section.

Isothermal chemical denaturation was performed by monitoring fluorescence both of intrinsic tryptophan residues by intrinsic tryptophan fluorescence (ITF) and of the exogenous fluorescence dye 1-anilinonaphthalene-8-sulfonate (ANS). Both polarity and dynamics of the tryptophan environment change upon denaturation as conformational transitions of the analyzed protein dramatically affect their fluorescence.[31] Most tryptophans are hidden from polar solvent in the hydrophobic core of proteins and thus show an emission maximum at ~330 nm, while the fully solvent-exposed tryptophan residues (upon denaturation of the protein) have their fluorescence maximum at ~355 nm. Furthermore, some of the tryptophans are close to the intra-domain disulfide bonds and thus are strongly quenched in the native state. The position of the emission maximum as well as the amplitude of fluorescence is thus both sensitive probes for monitoring conformational changes in antibodies. The analyzed IgG6B3 contains 26 tryptophanyl residues in its structure: each V_H/V_L pair contains 6, each C_H1/C_L 3, C_H2/C_H2 totally 4 and C_H3/C_H3 another 4 tryptophan residues.

On the other hand, ANS is a very weak fluorophore in polar solvents such as water and its

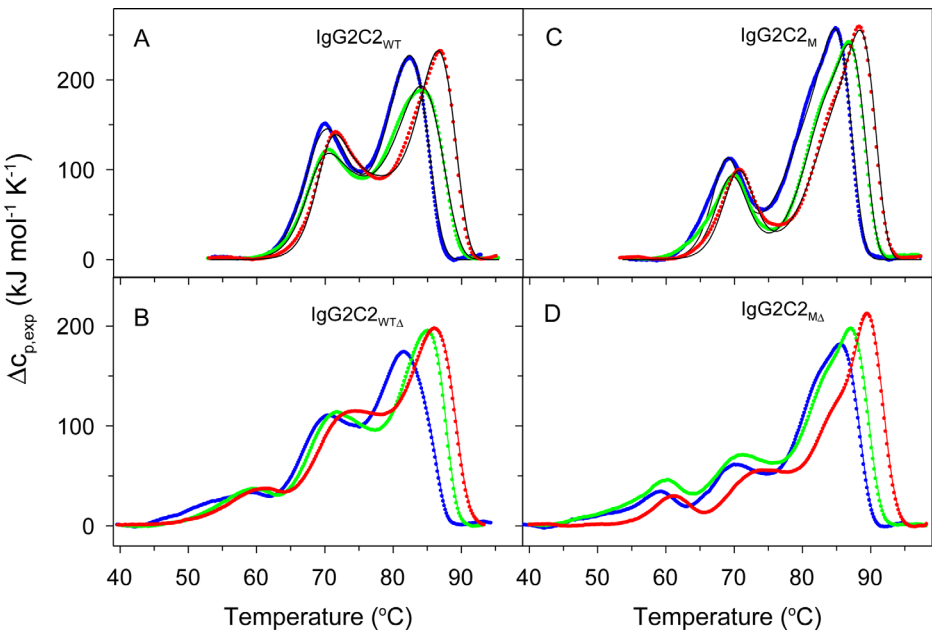

Figure 4. Thermal denaturations of IgG2C2s as a function of scan rate monitored by DSC: Data from (A) $IgG2C2_{WT}$, (B) $IgG2C2_{WT\Delta}$, (C) $IgG2C2_{M}$, (D) $IgG2C2_{M\Delta}$ indicate that these proteins are under kinetic control. Measurements were performed at three different scan rates: 0.5 K/min (blue), 1.0 K/min (green), and 1.5 K/min (red). Experimental data are shown as dots; theoretical fits based on a global fit according to Eq. (3) are shown as solid lines for $IgG2C2_{WT/M}$. DSC scans of non-glycosylated variants were not fitted to our model due to the complex nature of their thermal denaturations. Therefore, only experimental data are shown for the non-glycosylated variants of IgG2C2s. In all cases, DSC experiments were performed with 0.5 mg/mL of protein in PBS buffer, pH 7.4.

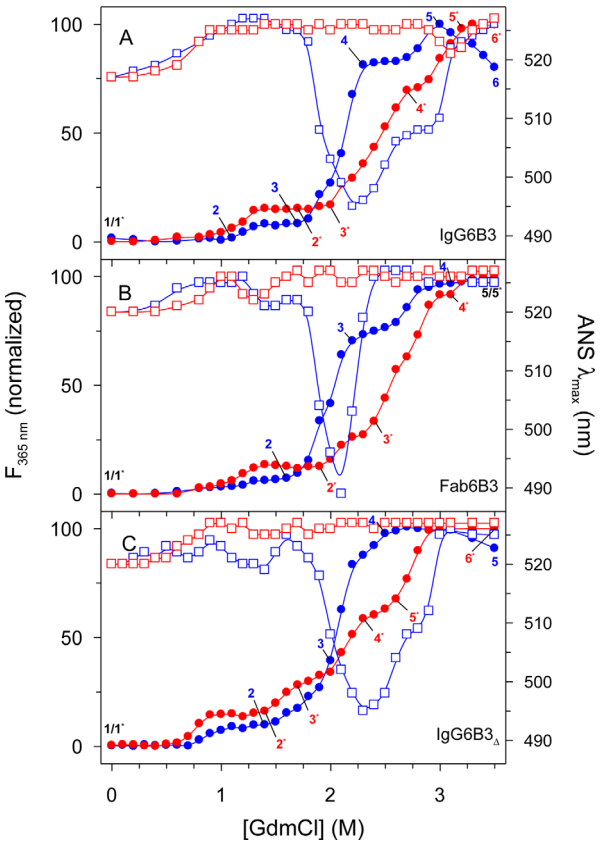

Figure 5. Isothermal denaturation of IgG6B3s and Fab6B3 fragments monitored by ITF (circles) and ANS fluorescence (squares) for wild type (blue) and engineered (red) variants: (A) $IgG6B3_{WT}$ and $IgG6B3_{M}$, (B) $Fab6B3_{WT}$ and $Fab6B3_{M}$, and (C) $IgG6B3_{WT\Delta}$ and $IgG6B3_{M\Delta}$. Numbers in the curves indicate positions of intermediate states detected from the phase diagram analysis (see Supporting information). Connecting lines serve only to lead the eye. All experiments were performed in PBS buffer, pH 7.4.

fluorescence significantly increases and shifts to shorter wavelengths in hydrophobic environments.[32,33] This feature causes a dramatic shift of its emission maximum upon binding of ANS to hydrophobic patches of partially un/folded protein molecules, thus allowing the detection of intermediate structures of IgG6B3s and Fab6B3s during isothermal denaturation with GdmCl.

The analyzed unfolding reactions of the studied proteins happen rather slowly. This observation is in agreement with previously published results,[34] stating that it took nearly a month of equilibration until no further changes in the denaturation curve could be observed. As equilibration of the unfolding reaction was not yet reached after 1 day incubation, we re-analyzed the samples again after 7 days incubation (Supporting Information Fig. S2). After 7 days, the intermediate states in protein unfolding can be more easily seen than in data recorded after only 1 day incubation at room temperature. Although the equilibrium has probably not been reached even after this extended incubation, for qualitative comparison and analysis of stabilization effect of mutations these recordings were sufficient.

The obtained data show that isothermal denaturation of all studied proteins, $IgG6B3_{WT/M}$, $Fab6B3_{WT/M}$ and $IgG6B3_{WT\Delta/M\Delta}$, is complex, as the transition of each protein consists of several intermediates (Fig. 5). However, the stabilizing effect of the mutations is clearly apparent for all engineered variants. This conclusion follows from a shift of denaturation curves to higher GdmCl concentrations in a concentration range between 2 and 3*M*. The distinct transition at ~1*M* GdmCl measured by Trp fluorescence (probably belonging to C_H2) is unaffected by the mutations (Fig. 5). Interestingly, the complexity of the isothermal unfolding of Fab6B3 fragments is comparable with that of the whole IgG, despite the missing homodimeric domains C_H2/C_H2 and C_H3/C_H3 [Fig. 5(B)]. This is likely a result of domain interactions between partially un/folded domains which can occur both in the isolated Fab6B3 fragment and the IgG6B3.

In contrast, ANS fluorescence clearly differentiates between intact IgG6B3s, that is, $IgG6B3_{WT}$ and $IgG6B3_{WT\Delta}$, and the $Fab6B3_{WT}$ fragment. For $IgG6B3_{WT}$ and $IgG6B3_{WT\Delta}$, ANS detects two apparent intermediate states as demonstrated by an emission maximum of ANS fluorescence at ~495 nm at ~2.2*M* GdmCl and ~505 nm at ~3*M* GdmCl [Fig. 5(A,C)], respectively. In the case of $Fab6B3_{WT}$, only one clearly defined intermediate at ~2*M* GdmCl with an emission maximum of ANS fluorescence at ~490 nm is detectable [Fig. 5(B)]. This observation either indicates that the intermediate at ~3*M* GdmCl is not part of the Fab6B3 fragment, or that an intermediate is formed which is stabilized by an interaction with the other domains. Interestingly, binding of ANS is not observed in isothermal unfolding of any protein containing the stabilizing mutations (red squares in Fig. 5).

The complexity of isothermal unfolding of studied IgG6B3 forms was also analyzed in phase diagrams.[35–38] The basis of this powerful method in revealing hidden intermediates is a pairwise correlation of two different independently extensive parameters (e.g., spectral intensities) in the same plot. For a two-state transition, the plot of the intensities should be linear, as each spectrum is a linear combination of the spectra of the two states. Any nonlinearity corresponds to the deviation from an all-or-none transition. The number of linear portions (n) indicates $n + 1$ species. This phase diagram method should be applied to data measured under identical conditions. Here, fluorescence emission intensities at 330 and 365 nm (upon excitation at 295 nm) were interrelated and plotted as F_{330} versus F_{365} (Supporting Information Figs. S3–S5). Clearly, the spectral diagrams are not linear, indicating the presence

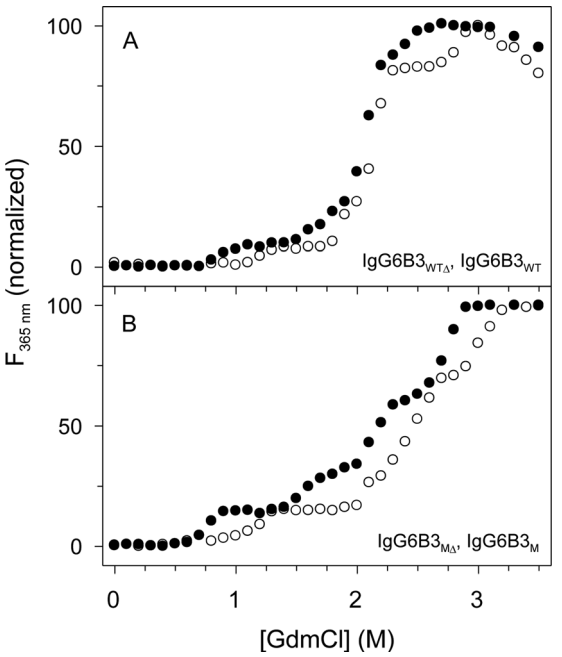

Figure 6. Effect of missing glycosylation on isothermal transitions of IgG6B3s monitored by ITF: (A) $IgG6B3_{WT}$ (white) and $IgG6B3_{WT\Delta}$ (black), and (B) $IgG6B3_{M}$ (white) and $IgG6B3_{M\Delta}$(black). All experiments were performed in PBS buffer, pH 7.4.

of intermediates and/or partially unfolded states. There are four/five linear regions which suggest at least five/six different species, indicated by numbers in Figure 5 and Supporting Information Figures S3–S5. Interestingly, the mutations just alter the position of intermediate states in the analyzed proteins but do not affect their number, pointing out that the mutations do not change the unfolding reactions — they 'only' stabilize the molecules against unfolding.

An intriguing conclusion follows from the comparison of unfolding curves of glycosylated and non-glycosylated forms of $IgG6B3_{WT}$ and $IgG6B3_{M}$ (Fig. 6). Deglycosylation in both proteins, $IgG6B3_{WT}$ and $IgG6B3_{M,}$ causes destabilization of the transition at $\sim$1*M* and $\sim$2.5*M* GdmCl. Surprisingly, in the case of $IgG6B3_{M}$ the absence of the glycan destabilizes all transitions. This observation might be interpreted as the inter- or intramolecular interaction of partially unfolded domains with each other, thereby stabilizing this partially unfolded state with respect to the pre-transition state.

Discussion

Immunoglobulins are multidomain proteins that usually show complex denaturation patterns when denatured either by high temperature or by denaturants. An often occurring complication in proper analyses of thermally and chemically induced denaturations of multidomain proteins is caused by the irreversible nature of the accompanying conformational changes. In such cases, thermodynamic and/or kinetic analyses of such transitions without justified models often lead to incorrect conclusions. In the present work, we studied thermally and chemically induced denaturation of wild-type and engineered IgGs and Fab fragments as well as non-glycosylated forms of the corresponding IgGs.

Analysis of thermal denaturations of antibodies

The analyses of thermal denaturation of Fab6B3 fragments were performed according to an already established model based on a one-step irreversible transition.[5,30] However, for the analyses of IgGs, we had to derive a new comprehensive model consisting of at least 3 observable transitions.

Thermal transitions of Fab6B3 fragments monitored by DSC consist of (i) single peaks (Fig. 2), (ii) depend on the used scan rate [Fig. 3(B)] and (iii) are irreversible—observations that are in agreement with previously published work.[18,26,39,40] These results provide a strong basis for the analysis of thermal denaturation according to a particular case of the Lumry-Eyring model, consisting of one irreversible step: $N \rightarrow F$, derived by Sanchez-Ruiz and colleagues.[5,30] The parameters obtained from these fits clearly show kinetic stabilization of the Fab fragment due to our mutations in the V_H domain (Table I). This is demonstrated by a $\sim$10,000-fold extension of the theoretical half-life of $Fab6B3_{M}$ at 37°C in comparison to $Fab6B3_{WT}$.

The thermally induced transitions of the whole IgGs, both for IgG6B3 and IgG2C2, are more complex but still can be expressed by the scheme represented by Eq. (1). This model is in agreement with conclusions of the work of Ionescu et al.[9] where the authors—based on the study of stability of humanized IgG_1—concluded that DSC profiles of IgG_1 generally consist of 2 or 3 visible peaks representing unfolding of domains in the following order: C_H2 < Fab < C_H3 (except for the rare cases of IgGs with extreme Fab stabilities, where they can overlap with C_H2 at the low end or C_H3 at the high end). The newly derived equation (Eq. (3)) for calculating the excess heat capacity enabled us to obtain fitting parameters that characterize all individual transitions of IgG thermal denaturation.

The parameters indicate that the mutations in the Fab6B3 fragment do not influence the first and the third transitions, that is, the unfolding of C_H2 and C_H3 domains, respectively. In fact, this is exactly what one would expect considering the location of the mutations at the "tip" of the Fab fragment. Interestingly, however, the kinetic stability of all analyzed Fab fragments *decreased* when they were part of the corresponding full-length IgG6B3. However, while for $Fab6B3_{WT}$ it decreased by $\sim$4 orders of magnitude, the kinetic stability was reduced only by $\sim$2 orders of magnitude for $Fab6B3_{M}$. This suggests that the partially

unfolded Fab fragments may interact with each other, as they do not seem to influence the denaturation of either C_H2 or C_H3, yet behave differently in the IgG than in isolation. Furthermore, the engineering of the Fab fragments, which had originally also been motivated by decreasing aggregation tendency and improving expression in *E. coli*,[24] may also be effective in the context of the IgG, and therefore make the engineered Fabs in the context of the IgG behave more like in isolation. Consequently, the combination of the higher intrinsic kinetic stability of $Fab6B3_M$ and its smaller decrease upon incorporation into IgG6B3 results in a ~6 orders of magnitude higher kinetic stability of $IgG6B3_M$ than that of $IgG6B3_{WT}$ (Table I) at 37°C.

Interestingly, the relative stabilizing effect of the mutations is similar also in IgG2C2 despite the different light chain classes in in these antibodies. The different composition of these Fab fragments is apparently the reason of the different (overall) kinetic stabilities of IgG2C2 and IgG6B3 (Table I). Indeed, the thermal denaturations of the C_H2 and C_H3 domains in IgG2C2 and IgG6B3 are described by similar parameters. The obtained very similar fitting parameters for C_H2 and C_H3 transitions despite the relatively dissimilar thermal transitions of full-length wild type and mutated IgG6B3 and IgG2C2 indicate the robustness of our model.

Analogous quantitative analyses of non-glycosylated IgGs, however, could not be performed by our model. In the case of non-glycosylated IgG6B3, the fitting was significantly worse for both $IgG6B3_{WT\Delta}$ and $IgG6B3_{M\Delta}$, indicating an incompatibility of our model with the thermal denaturations of these forms of IgG6B3 [Figs. 3(C,F)]. Applying a different model, for example, three consecutive irreversible transitions, did not significantly improve the fits (data not shown). Analyses of thermal denaturations of $IgG2C2_\Delta$ clearly show that the thermal denaturation of these variants proceed through more than 3 steps [Figs. 4(B,D)]. The appearance of another transition(s) in thermal denaturation of non-glycosylated IgGs can in principle indicate either destabilization of the full-length IgGs by missing glycosylation with concomitant additional intramolecular association reactions or inhomogeneity in the purified fraction of the protein. However, studies of the effects of the lack of glycosylation on the stability of Fc fragments[41,42] as well as of intact IgGs[43,44] are in qualitative consent with our results and indicate destabilization of C_H2 domains with additional small effects on the thermal stability of Fab region and C_H3 domains.[25] While some observations indicate only subtle modification of IgG stability due to the absent glycosylation,[43,44] in our hands, the destabilization of the first transition, the unfolding of the C_H2 domain, is quite significant. The temperatures of unfolding of the C_H2 domains decreased by ~7–10°C for the studied IgGs.

Analysis of isothermal denaturations of IgG6B3 antibodies

Isothermal denaturation curves can be analyzed only qualitatively due to their high complexity, extremely slow equilibration, and possibility of irreversibility under the experimental conditions. However, the conclusion that one can draw from our kinetic measurements is in agreement with the corresponding thermal denaturation data, that is, that the stability of IgG6B3 domains follow the order (from low to high stability) of C_H2 < Fab < C_H3. The first transition observed at GdmCl concentration of ~1*M* is a result of the unfolding of the C_H2 homodimeric domain, although one cannot exclude a contribution of the fluorescence signal from the Fab6B3 fragment. The former conclusion is strongly supported by the fact that non-glycosylated IgGs exhibit a destabilization of this transition [Figs. 5(A,C) and Fig. 6]. The latter conclusion is (at the same time) confirmed by the observation that unfolding of Fab6B3 fragments also contains a small transition in this concentration range [Fig. 5(B)]. A set of transitions between ~1.5*M* and 3.0*M* GdmCl corresponds to an unfolding of the Fab region, as clearly follows from the unfolding of Fab6B3 fragment shown in Figure 5(B). Finally, the unfolding of the C_H3 domains very likely proceeds at GdmCl concentrations >2.5*M*. This may be concluded from the following observations: (i) the existence of the intermediate state at ~2.8*M* GdmCl present in the intact IgG6B3 but absent in the Fab6B3 unfolding as detected by ANS fluorescence (Fig. 5) and (ii) the destabilization of the transitions of $IgG6B3_{WT\Delta/M\Delta}$ at >2.5*M* compared to $IgG6B3_{WT/M}$, due to the lack of glycosylation. Thus, absent glycosylation in C_H2 domains and its subsequent destabilization very likely affects also the stability of the closest protein region, the C_H3 domains, possibly by interactions between partially un/folded domains.

Glycosylation

Non-glycosylated forms of IgG have been produced in order to reduce effector functions, and thus to limit toxicity of some clinical candidates, such as, for example, otelixizumab (anti-CD3 IgG_1),[45] clazakizumab (BMS-945429, ALD518) (anti-IL-6 IgG_1),[46] BIIB-022 (anti-IGF-1R IgG_4).[47] Such non-glycosylated antibodies simplify bioprocessing, as glycan isoforms are avoided, but show a lower stability and higher aggregation tendency,[23,25,27,41,42,48] as analyzed by a new DSC approach in the present work.

This lower stability may be in part due to a destabilization of the C'E loop of the C_H2 domain in murine IgG_1[49] or the DE loop and FG loop in human

IgG_4.[50] While in wt C_H2 domains contacts between the domains are entirely mediated by the sugars, the absence of glycosylation apparently leads to more degrees of freedom for domain orientation, probably also contributing to a lower stability. In crystal structures of non-glycosylated Fc regions both open conformations and "super-closed" conformations have been found.[49–51] Measurements by small-angle X-ray scattering (SAXS) in solution suggest a more open orientation of the C_H2 domains for the non-glycosylated Fc.[51] The altered and/or disordered loop structures mentioned above are believed to contribute to the lack of Fcγ receptor binding and the reduced complement binding of non-glycosylated Fc regions,[52,53] while the structure still supports similar binding to the FcRn receptor and thus a long serum half-life in humans, as evident from the clinical trials cited above.

While in the Fc part, glycosylation at Asn297 has a clear biological function—supporting binding to FcγR and complement—spurious glycosylation may occur in the variable regions when they carry an accessible Asn-X-Ser/Thr motif.[53] It is even present in the marketed antibody cetuximab.[54] Fab glycosylation can lead to inconsistency of binding, depending on the expression host of the recombinant antibodies, and thus, modern antibody libraries have mostly removed such motifs, and the effect of V-domain glycosylation on stability—if any—has not been well investigated.

Conclusions

In summary, in this work we (i) suggest a novel model that accurately describes the thermal denaturation of IgG molecules and (ii) derive the equations in accordance with the model to apply them in numerical analyses of thermal denaturation of two different antibodies and their mutants, monitored by DSC. Our analyses confirmed and extended previous findings, that is, that the intact IgG undergoes thermal denaturation through three cooperative transitions corresponding to *reversible* denaturation of C_H2 domains followed by two consecutive *irreversible* transitions of Fab and C_H3 domains. Analyses of the fitting parameters of thermal denaturation of Fab6B3 fragments and the intact IgG6B3 variants suggest that individual domains apparently "feel" the presence of each other, potentially by un/folding intermediates interacting with each other.

In fact, kinetic parameters describing thermal unfolding of the individual Fab6B3 fragment and the IgG6B3 indicate that the Fab fragment is kinetically *destabilized* in the context of an IgG. Moreover, stabilizing mutations make the $Fab6B3_M$ fragment less sensitive towards the unfolding of other domains of the full-length antibody, possibly as a result of the lower abilities of the unfolded domains to affect the conformational state of the more stable Fab6B3 fragment. Thus, the mutations have a greater effect on the kinetic stability of the IgG than the corresponding Fab fragment.

We believe that applying the derived equation in the analyses of thermal denaturation of immunoglobulins, under the assumption that their thermal denaturation proceeds according to the suggested model, may provide improved information regarding de/stabilization effect of modification(s) in the protein structures of individual domains and/or due to different solvent formulations. This is currently investigated in a comprehensive study and will be presented in a different manuscript.

Acknowledgments

The authors thank Dr. Yuguang Zhao (Wellcome Trust Centre for Human Genetics, Oxford University) for his active help in IgG expression. They further thank Dr. Annemarie Honegger for her help in preparing Figure 1 and the other members of the Plückthun laboratory for fruitful discussions.

References

1. Beck A, Wurch T, Bailly C, Corvaia N (2010) Strategies and challenges for the next generation of therapeutic antibodies. Nat Rev Immunol 10:345–352.
2. Lumry R, Eyring H (1954) Conformation changes of proteins. J Phys Chem 58:110–120.
3. Lumry R, Biltonen R (1966) Validity of the "two-state" hypothesis for conformational transitions of proteins. Biopolymers 4:917–944.
4. Sanchez-Ruiz JM (2010) Protein kinetic stability. Biophys Chem 148:1–15.
5. Sanchez-Ruiz JM (1992) Theoretical analysis of Lumry-Eyring models in differential scanning calorimetry. Biophys J 61:921–935.
6. Sedlák E, Zoldák G, Wittung-Stafshede P (2008) Role of copper in thermal stability of human ceruloplasmin. Biophys J 94:1384–1391.
7. Sedlák E, Ziegler L, Kosman DJ, Wittung-Stafshede P (2008) In vitro unfolding of yeast multicopper oxidase Fet3p variants reveals unique role of each metal site. Proc Natl Acad Sci. U S A 105:19258–19263.
8. Sedlák E, Varhač R, Musatov A, Robinson NC (2014) The kinetic stability of cytochrome c oxidase: effect of bound phospholipid and dimerization. Biophys J 107: 2932–2940.
9. Ionescu RM, Vlasak J, Price C, Kirchmeier M (2008) Contribution of variable domains to the stability of humanized IgG1 monoclonal antibodies. J Pharm Sci 97:1414–1426.
10. Tischenko VM, Zav'yalov VP, Medgyesi GA, Potekhin SA, Privalov PL (1982) A thermodynamic study of cooperative structures in rabbit immunoglobulin G. Eur J Biochem 126:517–521.
11. Buchner J, Renner M, Lilie H, Hinz HJ, Jaenicke R, Kiefhaber T, Rudolph R (1991) Alternatively folded states of an immunoglobulin. Biochemistry 30:6922–6929.
12. Martsev SP, Kravchuk ZI, Vlasov AP, Lyakhnovich GV (1995) Thermodynamic and functional characterization of a stable IgG conformer obtained by renaturation from a partially structured low pH-induced state. FEBS Lett 361:173–175.

13. Vlasov AP, Kravchuk ZI, Martsev SP (1996) Non-native conformational states of immunoglobulins: thermodynamic and functional studies of rabbit IgG. Biochemistry (Moscow) 61:155–171.
14. Ejima D, Tsumoto K, Fukada H, Yumioka R, Nagase K, Arakawa T, Philo JS (2007) Effects of acid exposure on the conformation, stability, and aggregation of monoclonal antibodies. Proteins 66:954–962.
15. Kamerzell TJ, Ramsey JD, Middaugh CR (2008) Immunoglobulin dynamics, conformational fluctuations, and nonlinear elasticity and their effects on stability. J Phys Chem B 112:3240–3250.
16. Ahrer K, Buchacher A, Iberer G, Jungbauer A (2006) Thermodynamic stability and formation of aggregates of human immunoglobulin G characterised by differential scanning calorimetry and dynamic light scattering. J Biochem Biophys Methods 66:73–86.
17. Harn N, Allan C, Oliver C, Middaugh CR (2007) Highly concentrated monoclonal antibody solutions: direct analysis of physical structure and thermal stability. J Pharm Sci 96:532–546.
18. Shimba N, Torigoe H, Takahashi H, Masuda K, Shimada I, Arata Y, Sarai A (1995) Comparative thermodynamic analyses of the Fv, Fab* and Fab fragments of anti-dansyl mouse monoclonal antibody. FEBS Lett 360:247–250.
19. Vermeer AW, Norde W (2000) The thermal stability of immunoglobulin: unfolding and aggregation of a multidomain protein. Biophys J 78:394–404.
20. Manly SP, Matthews KS, Sturtevant JM (1985) Thermal denaturation of the core protein of lac repressor. Biochemistry 24:3842–3846.
21. Edge V, Allewell NM, Sturtevant JM (1985) High-resolution differential scanning calorimetric analysis of the subunits of Escherichia coli aspartate transcarbamoylase. Biochemistry 24:5899–5906.
22. Hu CQ, Sturtevant JM (1987) Thermodynamic study of yeast phosphoglycerate kinase. Biochemistry 26:178–182.
23. Schaefer JV, Plückthun A (2012) Transfer of engineered biophysical properties between different antibody formats and expression systems. Protein Eng Des Sel 25:485–506.
24. Ewert S, Huber T Honegger A, Plückthun A (2003) Biophysical properties of human antibody variable domains. J Mol Biol 325:531–553.
25. Liu H, Bulseco GG, Sun J (2006) Effect of posttranslational modifications on the thermal stability of a recombinant monoclonal antibody. Immunol Lett 106:144–153.
26. Garber E, Demarest SJ (2007) A broad range of Fab stabilities within a host of therapeutic IgGs. Biochem Biophys Res Commun 355:751–757.
27. Schaefer JV, Plückthun A (2012) Engineering aggregation resistance in IgG by two independent mechanisms: lessons from comparison of Pichia pastoris and mammalian cell expression. J Mol Biol 417:309–335.
28. Zoldák G, Zubrik A, Musatov A, Stupák M, Sedlák E (2004) Irreversible thermal denaturation of glucose oxidase from Aspergillus niger is the transition to the denatured state with residual structure. J Biol Chem 279:47601–47609.
29. Wakankar AA, Feeney MB, Rivera J, Chen Y, Kim M, Sharma VK, Wang YJ (2010) Physicochemical stability of the antibody-drug conjugate Trastuzumab-DM1: changes due to modification and conjugation processes. Bioconjug Chem 21:1588–1595.
30. Sánchez-Ruiz JM, López-Lacomba JL, Cortijo M, Mateo PL (1988) Differential scanning calorimetry of the irreversible thermal denaturation of thermolysin. Biochemistry 27:1648–1652.
31. Burstein EA, Vedenkina NS, Ivkova MN (1973) Fluorescence and the location of tryptophan residues in protein molecules. Photochem Photobiol 18:263–279.
32. Semisotnov GV, Rodionova NA, Razgulyaev OI, Uversky VN, Gripas' AF, Gilmanshin RI (1991) Study of the "molten globule" intermediate state in protein folding by a hydrophobic fluorescent probe. Biopolymers 31:119–128.
33. Hawe A, Sutter M, Jiskoot W (2008) Extrinsic fluorescent dyes as tools for protein characterization. Pharm Res 25:1487–1499.
34. Röthlisberger D, Honegger A, Plückthun A (2005) Domain interactions in the Fab fragment: a comparative evaluation of the single-chain Fv and Fab format engineered with variable domains of different stability. J Mol Biol 347:773–789.
35. Bushmarina NA, Kuznetsova IM, Biktashev AG, Turoverov KK, Uversky VN (2001) Partially folded conformations in the folding pathway of bovine carbonic anhydrase II: a fluorescence spectroscopic analysis. ChemBioChem 2:813–821.
36. Kuznetsova IM, Stepanenko OV, Turoverov KK, Zhu L, Zhou JM, Fink AL, Uversky VN (2002) Unraveling multistate unfolding of rabbit muscle creatine kinase. Biochim Biophys Acta 1596:138–155.
37. Kuznetsova IM, Turoverov KK, Uversky VN (2004) Use of the phase diagram method to analyze the protein unfolding-refolding reactions: fishing out the "invisible" intermediates. J Proteome Res 3:485–494.
38. Zoldák G, Sedlák E, Wolfrum A, Musatov A, Fedunová D, Szkaradkiewicz K, Sprinzl M (2008) Multidomain initiation factor 2 from Thermus thermophilus consists of the individual autonomous domains. Biochemistry 47:4992–5005.
39. Welfle K, Misselwitz R, Hausdorf G, Höhne W, Welfle H (1999) Conformation, pH-induced conformational changes, and thermal unfolding of anti-p24 (HIV-1) monoclonal antibody CB4-1 and its Fab and Fc fragments. Biochim Biophys Acta 1431:120–131.
40. Demarest SJ, Chen G, Kimmel BE, Gustafson D, Wu J, Salbato J, Poland J, Elia M, Tan X, Wong K, Short J, Hansen G (2006) Engineering stability into Escherichia coli secreted Fabs leads to increased functional expression. Protein Eng Des Sel 19:325–336.
41. Ghirlando R, Lund J, Goodall M, Jefferis R (1999) Glycosylation of human IgG-Fc: influences on structure revealed by differential scanning micro-calorimetry. Immunol Lett 68:47–52.
42. Mimura Y, Church S, Ghirlando R, Ashton PR, Dong S, Goodall M, Lund J, Jefferis R (2000) The influence of glycosylation on the thermal stability and effector function expression of human IgG1-Fc: properties of a series of truncated glycoforms. Mol Immunol 37:697–706.
43. Alsenaidy MA, Kim JH, Majumdar R, Weis DD, Joshi SB, Tolbert TJ, Middaugh CR, Volkin DB (2013) High-throughput biophysical analysis and data visualization of conformational stability of an IgG1 monoclonal antibody after deglycosylation. J Pharm Sci 102:3942–3956.
44. Alsenaidy MA, Okbazghi SZ, Kim JH, Joshi SB, Middaugh CR, Tolbert TJ, Volkin DB (2014) Physical stability comparisons of IgG1-Fc variants: effects of N-glycosylation site occupancy and Asp/Gln residues at site Asn 297. J Pharm Sci 103:1613–1627.
45. Aronson R, Gottlieb PA, Christiansen JS, Donner TW, Bosi E, Bode BW, Pozzilli P (2014) Low-dose otelixizumab anti-CD3 monoclonal antibody DEFEND-1 study: results of the randomized phase III study in recent-

onset human type 1 diabetes. DEFEND Investigator Group. Diabetes Care 37:2746–2754.
46. Mease P, Strand V, Shalamberidze L, Dimic A, Raskina T, Xu LA, Liu Y, Smith J (2012) A phase II, double-blind, randomised, placebo-controlled study of BMS945429 (ALD518) in patients with rheumatoid arthritis with an inadequate response to methotrexate. Ann Rheum Dis 71:1183–1189.
47. von Mehren M, Britten CD, Pieslor P, Saville W, Vassos A, Harris S, Galluppi GR, Darif M, Wainberg ZA, Cohen RB, Leong S (2014) A phase 1, open-label, dose-escalation study of BIIB022 (anti-IGF-1R monoclonal antibody) in subjects with relapsed or refractory solid tumors. Invest New Drugs 32:518–525.
48. Kayser V, Chennamsetty N, Voynov V, Forrer K, Helk B, Trout BL (2011) Glycosylation influences on the aggregation propensity of therapeutic monoclonal antibodies. Biotechnol J 6:38–44.
49. Feige MJ, Nath S, Catharino SR, Weinfurtner D, Steinbacher S, Buchner J (2009) Structure of the murine unglycosylated IgG1 Fc fragment. J Mol Biol 391:599–608.
50. Davies AM, Jefferis R, Sutton BJ (2014) Crystal structure of deglycosylated human IgG4-Fc. Mol Immunol 62:46–53.
51. Borrok MJ, Jung ST, Kang TH, Monzingo AF, Georgiou G (2012) Revisiting the role of glycosylation in the structure of human IgG Fc. ACS Chem Biol 7: 1596–1602.
52. Lund J, Takahashi N, Pound JD, Goodall M, Jefferis R (1996) Multiple interactions of IgG with its core oligosaccharide can modulate recognition by complement and human Fcγ receptor I and influence the synthesis of its oligosaccharide chains. J Immunol 157:4963–4969.
53. Hayes JM, Cosgrave EF, Struwe WB, Wormald M, Davey GP, Jefferis R, Rudd PM (2014) Glycosylation and Fc receptors. Curr Top Microbiol Immunol 382:165–199.
54. Ayoub D, Jabs W, Resemann A, Evers W, Evans C, Main L, Baessmann C, Wagner-Rousset E, Suckau D, Beck A (2013) Correct primary structure assessment and extensive glyco-profiling of cetuximab by a combination of intact, middle-up, middle-down and bottom-up ESI and MALDI mass spectrometry techniques. mAbs 5:699–710.

APPENDIX

The total enthalpy of the system $N \rightleftharpoons U \rightarrow D \rightarrow F$ (using state N as the reference level) is given by

$$\begin{aligned} H_{total}(T) &= (1-n_U-n_D-n_F)H_N(T)+n_U H_U(T) \\ &+n_D H_D(T)+n_F H_F(T) = H_N(T)+n_U \Delta H_U(T) \\ &+n_D \Delta H_D(T)+n_F \Delta H_F(T) \end{aligned} \tag{A1}$$

$$\begin{aligned} C_p(T) &= \frac{dH_{total}(T)}{dT} = \frac{dH_N(T)}{dT} + n_U \frac{d\Delta H_U(T)}{dT} \\ &+n_D \frac{d\Delta H_D(T)}{dT} + n_F \frac{d\Delta H_F(T)}{dT} + \Delta H_U(T)\frac{dn_U}{dT} \\ &+\Delta H_D(T)\frac{dn_D}{dT} + \Delta H_F(T)\frac{dn_F}{dT} \end{aligned} \tag{A2}$$

$$C_p(T) = baseline(T) + C_p^{excess}(T) \tag{A3}$$

where

$$baseline(T) = C_p^N(T) + n_U \Delta C_p^U(T) + n_D \Delta C_p^D(T) + n_F \Delta C_p^F(T) \tag{A4}$$

$$C_p^{excess}(T) = \Delta H_U(T)\frac{dn_U}{dT} + \Delta H_D(T)\frac{dn_D}{dT} + \Delta H_F(T)\frac{dn_F}{dT} \tag{A5}$$

and

$$\begin{aligned} &\Delta H_x(T) = H_x(T) - H_N(T) \\ &\Delta C_p^x(T) = C_p^x(T) - C_p^N(T) \\ &\Delta H_x(T) \approx \Delta H_x(T_{ref}) + \Delta C_p^x(T_{ref})\,(T - T_{ref}) \\ &\Delta C_p^x(T) \approx \Delta C_p^x(T_{ref}) + const_x\,(T - T_{ref}) \\ &x \in \{U, D, F\} \\ &n_N + n_U + n_D + n_F = 1 \\ &\Delta H_U(T) = \Delta H_1(T);\quad \Delta H_D(T) = \Delta H_1(T) + \Delta H_2(T);\quad \Delta H_F(T) = \Delta H_1(T) + \Delta H_2(T) + \Delta H_3(T) \end{aligned} \tag{A6}$$

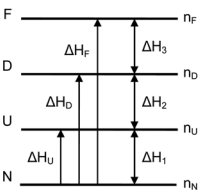

From Eq. (A5) and Eq. (A6), neglecting the temperature dependence of $\Delta H_x(T)$

$$\begin{aligned} C_p^{excess}(T) &= \Delta H_1\left(\frac{dn_U}{dT} + \frac{dn_D}{dT} + \frac{dn_F}{dT}\right) \\ &+\Delta H_2\left(\frac{dn_D}{dT} + \frac{dn_F}{dT}\right) + \Delta H_3\left(\frac{dn_F}{dT}\right) = \end{aligned}$$

changing the reference level

$$\begin{aligned} &= \Delta H_1 \frac{d(1-n_N)}{dT} + \Delta H_2 \frac{d(1-n_N-n_U)}{dT} \\ &+\Delta H_3 \frac{d(1-n_N-n_U-n_D)}{dT} = -\Delta H_1\left(\frac{dn_N}{dT}\right) \\ &-\Delta H_2\left(\frac{dn_N}{dT} + \frac{dn_U}{dT}\right) - \Delta H_3\left(\frac{dn_N}{dT} + \frac{dn_U}{dT} + \frac{dn_D}{dT}\right) = \end{aligned}$$

using a system of differential equations describing the model $N \underset{k_{-1}}{\overset{k_1}{\rightleftharpoons}} U \xrightarrow{k_2} D \xrightarrow{k_3} F$

$$\begin{aligned} \frac{dn_N}{dT} &= \frac{1}{v}(-k_1 n_N + k_{-1} n_U) \\ \frac{dn_U}{dT} &= \frac{1}{v}\left(k_1 n_N - (k_{-1}+k_2) n_U\right) \\ \frac{dn_D}{dT} &= \frac{1}{v}(k_2 n_U - k_3 n_D) \\ \frac{dn_F}{dT} &= \frac{1}{v}(k_3 n_D) \end{aligned} \tag{A7}$$

yields

$$= -\Delta H_1\left(\frac{dn_N}{dT}\right) - \Delta H_2\left(\frac{-k_2 n_U}{v}\right) - \Delta H_3\left(\frac{-k_2 n_U}{v} + \frac{k_2 n_U - k_3 n_D}{v}\right)$$

and finally

$$C_p^{excess}(T) = -\Delta H_1\left(\frac{dn_N}{dT}\right) + \Delta H_2\left(\frac{k_2 n_U}{v}\right) + \Delta H_3\left(\frac{k_3 n_D}{v}\right) \tag{A8}$$

The first two equations (A7) are independent relative to the other and in such a way can be solved separately, in two steps described by two consecutive reactions:

$$\text{Reaction 1}: \quad N \overset{K}{\rightleftharpoons} U \xrightarrow{k_2}$$

$$\text{Reaction 2}: \quad \xrightarrow{k_2} D \xrightarrow{k_3} F$$

with corresponding molar heat capacities for reactions are expressed as:

$$\text{For reaction 1}: \quad C_{p,reaction\,1}^{excess}(T) = -\Delta H_1\left(\frac{dn_N}{dT}\right)$$

$$\text{For reaction 2}: \quad C_{p,reaction\,2}^{excess}(T) = \Delta H_2\left(\frac{k_2 n_U}{v}\right) + \Delta H_3\left(\frac{k_3 n_D}{v}\right)$$

The corresponding fractional occupancies of states in Reaction 1, N and U are given by Sanchez-Ruiz:[5]

$$\begin{aligned} n_N &= \frac{1}{K+1}\varepsilon_K \\ n_U &= \frac{K}{K+1}\varepsilon_K \end{aligned} \tag{A9}$$

where

$$\begin{aligned} \varepsilon_K &= \exp\left(-\frac{1}{v}\int \frac{k_2 K}{K+1} dT\right) \\ K = \frac{k_1}{k_{-1}} &= \exp\left(-\frac{\Delta H_1}{R}\left(\frac{1}{T} - \frac{1}{T_{1/2}}\right)\right) \\ k_2 &= \exp\left(-\frac{E_{a2}}{R}\left(\frac{1}{T} - \frac{1}{T_2^*}\right)\right) \end{aligned} \tag{A10}$$

The fractional occupancy of state n_D in Reaction 2 is given by third differential equation from system (A7):

$$\frac{dn_D}{dT} + \frac{1}{v}k_3 n_D = \frac{1}{v}k_2 n_U \tag{A11}$$

where n_U is taken from Eq. (A9). Eq. (A11) represents a nonhomogenous linear differential equation, which is solved by a general method as follows: looking for a solution in the form

$$n_D = n_D^0(T)\exp\left(-\frac{1}{v}\int k_3 dT\right) = n_D^0(T)\varepsilon_3 \tag{A12}$$

where ε_3 in Eq. (A12) represents the solution of a homogenous differential equation

$$\frac{dn_D}{dT} + \frac{1}{v}k_3 n_D = 0$$

gives the expression for the fractional occupancy of D-state, n_D:

$$n_D = \frac{\varepsilon_3}{v}\int\left(\frac{k_2 K}{K+1}\frac{\varepsilon_K}{\varepsilon_3}\right)dT \tag{A13}$$

Substituting the obtained values for fractional occupancies of the states N, U and D into equation for the excess heat capacity (Eq. (A8)) describing the thermal transitions according the model (Eq. (A7)) gives us a final equation:

$$\begin{aligned} C_p^{excess}(T) = \Delta H_1 \frac{K}{(K+1)^2}\left(\frac{k_2}{v} + \frac{\Delta H_1}{RT^2}\right)\varepsilon_K + \\ \Delta H_2 \frac{K}{K+1}\left(\frac{k_2}{v}\right)\varepsilon_K + \Delta H_3 \frac{k_3}{v^2}\varepsilon_3 \int\left(\frac{k_2 K}{K+1}\frac{\varepsilon_K}{\varepsilon_3}\right)dT \end{aligned} \tag{A14}$$

Here ε_K, K and k_2 are defined by Eq. (A10) and k_3 and ε_3 are defined as follows:

$$k_3 = exp\left(-\frac{E_{a3}}{R}\left(\frac{1}{T} - \frac{1}{T_3^*}\right)\right)$$

$$\varepsilon_3 = exp\left(-\frac{1}{v}\int k_3 dT\right)$$